

From the topological spin-Hall effect to the non-Hermitian skin effect in an elliptical micropillar chain

S. Mandal,^{*} R. Banerjee,[†] and T.C.H. Liew[‡]

*Division of Physics and Applied Physics, School of Physical and Mathematical Sciences,
Nanyang Technological University, Singapore 637371, Singapore*

The topological spin-Hall effect causes different spins to propagate in opposite directions based on Hermitian physics. The non-Hermitian skin effect causes the localization of all modes of a system at its edges. Although these effects have separately attracted tremendous interest, their completely different origins have made them hard to observe in a single system. Here we propose a system based on exciton-polariton elliptical micropillars hosting both the effects. The polarization splitting and different orientation of the elliptical micropillars naturally give rise to the topological spin-Hall effect in a one dimensional lattice. By making the effective decay rates of the different spin (σ_{\pm}) modes unequal, the system makes a phase transition from the Hermitian regime to non-Hermitian regime showing the non-Hermitian skin effect.

Introduction.— The field of topological insulators (TIs) started with the discovery of the quantum Hall effect [1] followed by the Haldane model [2], where electrons propagate robustly along the edges of a finite 2D sample. Later, Kane and Mele came up with the spin dependent version of the Haldane model, where they predicted that electrons with different spins would propagate robustly in opposite directions [3]. This is known as the topological spin-Hall effect (TSHE), which is expected to play an important role in the field of spintronics [4].

In the last decade, the concept of TIs has not only been extended from fermions to different bosonic systems such as photonics [5–9] and acoustics [10], but higher order TIs have also been demonstrated in those systems [11–15]. In photonic system the role of spins can be played by the photonic circular polarizations (σ_{\pm}). However, due to the presence of the splitting in energy between the transverse-electric (TE) and transverse-magnetic (TM) modes (which effectively couples the σ_{\pm} polarizations), realizing the TSHE for photons is far from trivial and often needs extremely careful fabrication in order to reduce the TE-TM splitting [16]. Instead of the photonic polarization, if the role of spin is played by an external degree of freedom such as the angular momentum [17–19] or valley degree of freedom [20–22], then realizing the TSHE in photonic systems is more readily achieved.

Recently, non-Hermitian topological phases, especially the non-Hermitian skin effect (NHSE), has been an intense area of research. Typically in a finite 1D lattice if the coupling between the adjacent sites is made different in the forward and backward directions (non-reciprocal coupling), then all the modes of the system get localized at the edges of the finite lattice leaving no modes located in the bulk [23–28]. This is unlike the topologically non-trivial Hermitian systems, where the number of edge modes residing within the bulk band gaps is de-

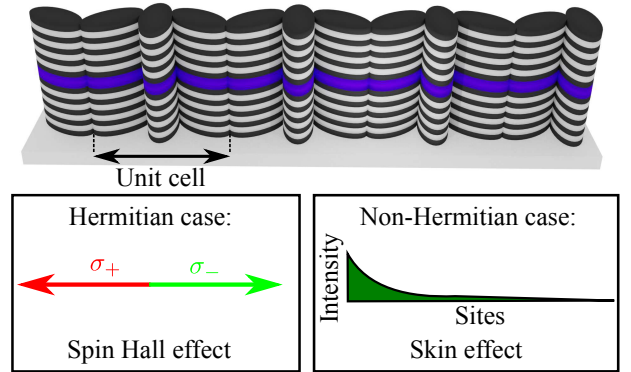


FIG. 1: Schematic of an exciton-polariton elliptical micropillar chain. Proper orientations of the elliptical micropillars naturally give rise to the spin-Hall effect. If the polaritons having opposite circular polarizations (σ_{\pm}) have unequal decay rates, the non-Hermitian skin effect appears.

termined by the bulk-edge correspondence [29]. Due to the exotic edge localization, any injected signal, independent of its excitation position, always propagates in one direction while the propagation in the opposite direction is strongly suppressed [25, 30]. Such an effect can be extremely useful in suppressing feedback in optical circuits, which is a necessity [31]. However, achieving the non-reciprocal coupling between two sites in an optical system is difficult and often requires complicated experimental setups, which are hard to be integrated into micro/nano-scale [30].

Exciton-polaritons are quasiparticles arising due to the strong coupling of cavity photons and quantum well excitons [32]. Their fascinating properties, such as finite lifetime, sensitivity to external fields, strong non-linearity inherited from excitons, spin polarizations, etc, make them ideal for studying both the Hermitian and non-Hermitian topological phases. The polariton Chern insulator in presence of Zeeman splitting and TE-TM splitting has been studied theoretically [33–41] and realized experimentally [42]. Nonlinear topological polaritons have also been an intense area of research [43–46],

^{*}Corresponding author: subhaska001@e.ntu.edu.sg

[†]Corresponding author: rimi001@e.ntu.edu.sg

[‡]Corresponding author: tchliew@gmail.com

where in some cases the nonlinearity alone induces topological behavior [47–50]. The inherent non-Hermitian nature of the polaritons has led to the realization of exceptional points [51, 52], non-Hermitian topological phases [52, 53], and other related theoretical predictions [54–56]. The spin-orbit coupling due to the TE-TM splitting inside the microcavity has played a vital role in obtaining nontrivial spin related effects, such as the optical spin Hall effect [57–59], meron polarization textures [65], nontrivial bands with spin orbit interaction Hamiltonians [60–67].

In this work, we propose a system based on an exciton-polariton elliptical micropillar chain, where both the TSHE and NHSE can be realized in a single set up (see Fig. 1). By proper orientation of the otherwise identical elliptical micropillars along with the naturally present polarization splitting due to the shape anisotropy give rise to a band structure, where the positive and negative momentum states have opposite circular polarizations (σ_{\pm}). As a result σ_{\pm} polaritons propagate in the opposite directions in the chain giving rise to the TSHE. If the effective decay rates of the σ_{\pm} polaritons are made unequal by subjecting the chain to a circularly polarized spatially uniform incoherent pump, the non-Hermitian physics takes over. The behavior of the system changes drastically and the modes of the system get localized at one end of the chain, giving rise to the NHSE [23], where σ_{\pm} polaritons propagate in the same direction, while the propagation in the other direction is strongly suppressed. The key advantage of our scheme is that here both the topological Hermitian and non-Hermitian phases can be studied on the same sample without the need of spatial patterning of the pump. Besides the robust polariton propagation here is in a one dimensional lattice, which is more compact and ideal for potential information transport applications.

Topological spin-Hall effect.— In order to show the TSHE, we first consider a square lattice, which is periodic along the x direction and has N_y sites along the y direction (see Fig. 2(a)). The coupling between the nearest sites along the x direction is taken as J , while the coupling between the nearest sites along the y direction is taken as complex $\Delta e^{in_x\phi}$, where n_x is the site number along the x direction. The total phase in each plaquette becomes ϕ ($-\phi$) while hopping counter-clockwise (clockwise). Any nonzero phase ϕ introduces an effective magnetic field, which breaks the time reversal (TR) symmetry in the system. The Hamiltonian of the system can be represented as

$$\hat{H} = \sum_{n_x, n_y} \left[-J \hat{a}_{n_x, n_y}^{\dagger} \hat{a}_{n_x+1, n_y} + \Delta e^{in_x\phi} \hat{a}_{n_x, n_y}^{\dagger} \hat{a}_{n_x, n_y+1} \right] + \text{h.c.} \quad (1)$$

Here n_y is the site index along the y direction, $\hat{a}_{n_x, n_y}^{\dagger}$ (\hat{a}_{n_x, n_y}) is the particle creation (annihilation) operator at site (n_x, n_y) , and h.c. represents the Hermitian conjugate. The Hamiltonian in Eq. (1) gives rise to the

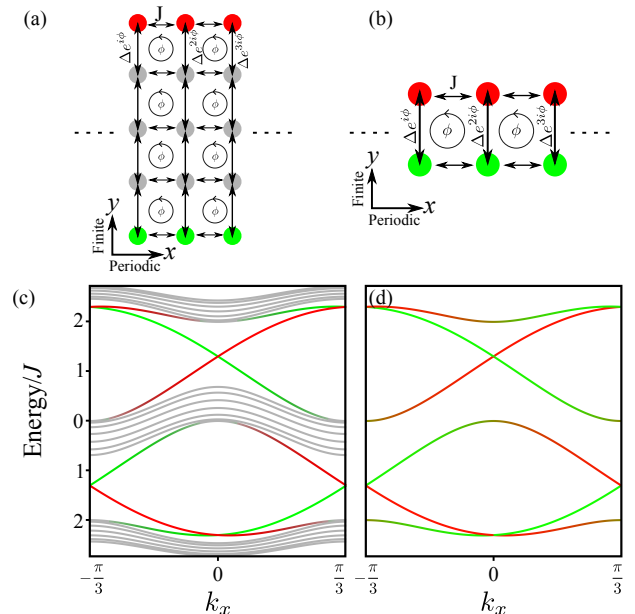


FIG. 2: (a) The unit cell of a square lattice with real couplings along the x direction and complex couplings along the y direction such that each plaquette has total accumulated phase $\phi = 2\pi/3$. (b) The same lattice as in (a), but having only two sites along the y direction. (c-d) The band structure of the system presented in (a-b), respectively. The bulk bands are shown in grey, whereas red and green being the edge states located at the opposite edges. Parameters: $\Delta/J = 1$.

Hofstadter butterfly if the eigenenergies of the system are plotted against ϕ [17, 68], where for $\phi = 2\pi/q$, each Bloch band splits into q sub-bands. In Fig. 2(a) the unit cell of the system, which is periodic along the x direction, is shown for $\phi = 2\pi/3$. The band structure of the system is shown in Fig. 2(c), where the bulk bands are shown in grey, while red and green represent the edge states located at the two edges. As expected there are three bulk bands, which are connected by the topologically protected edge states.

Next, we reduce the width of the lattice and keep only two sites along the y direction (see Fig. 2(b)). The band structure of such a lattice is shown in Fig. 2(d). Remarkably the band structure in this case is exactly the same as the one Fig. 2(c), however all the bulk modes disappear leaving behind only the edge modes. Achieving complex hopping between sites for polaritons is extremely challenging, which makes the realization of the system shown in Fig. 2(a) difficult in practice. However, considering the red (green) sites as σ_+ (σ_-) spin states of the polaritons, the system shown in Fig. 2(b) can be mapped to a chain of elliptical micropillars (see Fig. 3(a)), where Δ is the polarization splitting inside the micropillars due to shape anisotropy [69] and ϕ represents the orientation angle. With this interpretation the system becomes TR symmetric and red (green) represents the σ_+ (σ_-) spin states in the band structure in Fig. 2(d). The states having positive and negative momentum have opposite

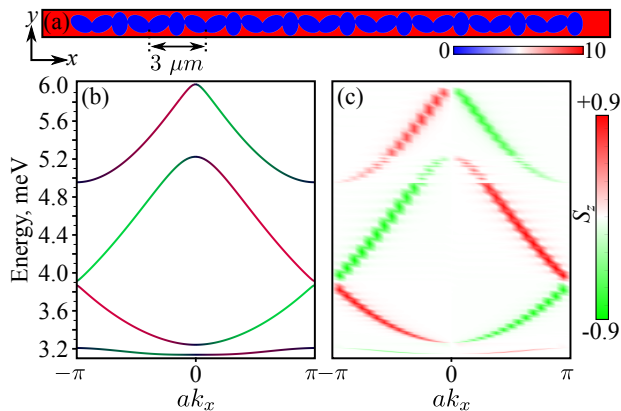


FIG. 3: (a) A chain of elliptical micropillars, where three pillars oriented by $\pi/3$ with respect to each other form an unit cell. (b-c) Band structure of the system under consideration using Bloch theorem (infinite chain) and by Fourier transforming the eigenstates of a finite chain.

circular polarizations. As a result σ_{\pm} spins propagate in the opposite directions giving rise to the TSHE.

The complex hopping between the σ_{\pm} states inside an elliptical micropillar can be shown using a basis transformation, where an orientation angle θ induces 2θ phase in the hopping term [70]. The dynamics of the polaritons in a chain of elliptical micropillars can be described by the following driven-dissipative Gross-Pitaevskii equation

$$i\hbar \frac{\partial \psi_{\sigma_{\pm}}}{\partial t} = \left[-\frac{\hbar^2 \nabla^2}{2m} + V(x, y) + i(P_{\sigma_{\pm}} - \Gamma) \right] \psi_{\sigma_{\pm}} + V_T(x, y, \theta) \psi_{\sigma_{\mp}} + F_{\sigma_{\pm}}(x, y) e^{i(k_p x - \omega_p t)}. \quad (2)$$

Here ∇^2 represents the Laplacian, $m = 7.5 \times 10^{-5} m_e$ is the polariton mass with m_e being the free electron mass. V represents the potential corresponding to the chain of elliptical micropillars shown in Fig. 3(a) with potential depth 10 meV. In order to realize $2\pi/3$ phase in each plaquette (see Fig. 2(b)), any two neighbouring elliptical micropillars need to be oriented by an angle $\pi/3$ with respect to each other. To be consistent with experiment we choose the micropillars having semi-major axis $1.3 \mu\text{m}$ and semi-minor axis $0.85 \mu\text{m}$ [69], which gives a three micropillar unit cell with length $a = 3 \mu\text{m}$. $P_{\sigma_{\pm}}$ is the gain corresponding to an incoherent pump and $\Gamma = 0.032$ meV represents the polariton decay corresponding to a lifetime around 10 ps. V_T represents the linear polarization splitting around 1 meV inside the pillars [69], which has the same spatial profile as V but multiplied by a factor $e^{\pm 2i\theta}$ corresponding to the orientation of each micropillars. $F_{\sigma_{\pm}}$ is a coherent pump that serves to inject polaritons having energy $\hbar\omega_p$ and wave vector k_p .

In Fig. 3(b) we remove the pump and decay terms ($P_{\sigma_{\pm}} = \Gamma = F_{\sigma_{\pm}} = 0$) and calculate the band structure of the system using the Bloch theorem. The band structure is similar to the one in Fig. 2(d) with the positive and negative momentum states having opposite circular

polarizations. In Fig. 3(c) the same band structure is obtained by Fourier transforming the eigenstates of a finite chain, which corresponds to the photoluminescence spectrum in the experiments. The colorbar corresponds to the degree of circular polarization, which is defined as $S_z = (|\psi_{\sigma_+}|^2 - |\psi_{\sigma_-}|^2) / (|\psi_{\sigma_+}|^2 + |\psi_{\sigma_-}|^2)$.

In order to see the effect of the TSHE, we consider $\Gamma \neq 0$, $F_{\sigma_{\pm}} \neq 0$ keeping $P_{\sigma_{\pm}} = 0$. The polaritons are injected using a tightly localized linearly polarized Gaussian shaped coherent continuous pump positioned at the middle of the chain. The full width at half maximum of the pump is around $2.1 \mu\text{m}$, which excites a wide range of momentum corresponding to a particular energy. In Fig. 4(a-b) the dynamics of the σ_{\pm} polaritons are shown, where they propagate in the opposite directions showing the TSHE. This is expected from the band structure as σ_{\pm} states have opposite group velocities. The intensity of the polaritons decreases with the propagation distance due to their finite lifetime. Fig. 4(c) shows the degree of circular polarization of the propagating polaritons. The full dynamics of the polariton under a linearly polarized coherent pump and pulse is shown in movie1 [70]. Such non-trivial propagation of polariton spins exists for an energy range around 1.5 meV (3.3 - 4.8 meV; above this the propagation direction for σ_{\pm} polaritons changes). This is around 15 times larger than the non-trivial bandgap of the topological polaritons observed in [42].

Non-Hermitian skin effect.— Until now the dynamics of the polaritons were determined by the Hermitian physics, with the non-Hermitian decay term determining the rate of loss of intensity with a factor $e^{-2\Gamma t}$. Here we choose different decay rates corresponding to the σ_{\pm} modes. The Hamiltonian in Eq. (1) gets updated to

$$\hat{H} = -J \sum_{n_x, \sigma_{\pm}} \left[\hat{a}_{n_x, \sigma_{\pm}}^{\dagger} \hat{a}_{n_x+1, \sigma_{\pm}} + \hat{a}_{n_x+1, \sigma_{\pm}}^{\dagger} \hat{a}_{n_x, \sigma_{\pm}} \right] + \sum_{n_x, \sigma_{\pm}} \left[\Delta e^{\pm i n_x \phi} \hat{a}_{n_x, \sigma_{\pm}}^{\dagger} \hat{a}_{n_x, \sigma_{\mp}} - i\Gamma_{\sigma_{\pm}} \hat{a}_{n_x, \sigma_{\pm}}^{\dagger} \hat{a}_{n_x, \sigma_{\pm}} \right]. \quad (3)$$

Here $\Gamma_{\sigma_{\pm}}$ are the effective decay rates of the σ_{\pm} modes. We choose $\Gamma_{\sigma_+} < \Gamma_{\sigma_-}$ and diagonalize the Hamiltonian having 90 sites along the x axis (see Fig. 5(a)). The spatial profiles of all the modes corresponding to both σ_{\pm} spins are plotted in Fig. 5(b-c). The modes having real energy < 0 (> 0) are localized at the left (right) end of the lattice. This is known as the NHSE, where whole band collapse to one end of the finite lattice. Unlike the TSHE, where the σ_{\pm} spins propagate in opposite directions, here both the σ_{\pm} spins are localized at the same end. σ_{\pm} polaritons propagate in opposite directions. When σ_+ polaritons hit the end of the chain, they couple to counter-propagating σ_- modes. However, since $\Gamma_{\sigma_+} < \Gamma_{\sigma_-}$, the σ_- modes decay (much faster compared to σ_+ modes) before propagating a significant distance. Due to this a large population of the polaritons builds up at the end of the chain giving rise to the non-Hermitian

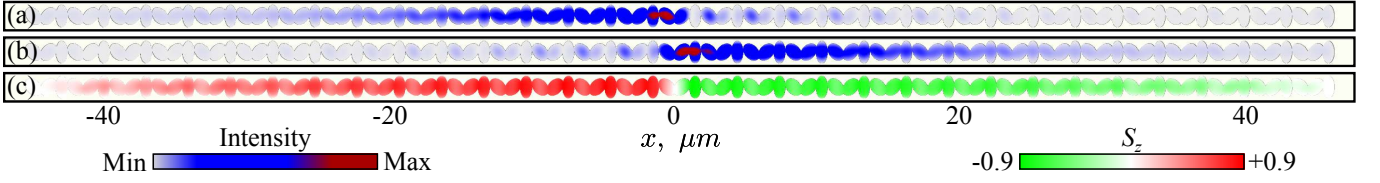


FIG. 4: Topological spin-Hall effect: (a-c) $|\psi_{\sigma_{\pm}}|^2$, and S_z , respectively, at $t = 60$ ps under a linearly polarized coherent pump positioned at the middle ($x = 0 \mu\text{m}$) of the chain. Parameters: $\hbar\omega_p = 3.6$ meV and $ak_p = 0$.

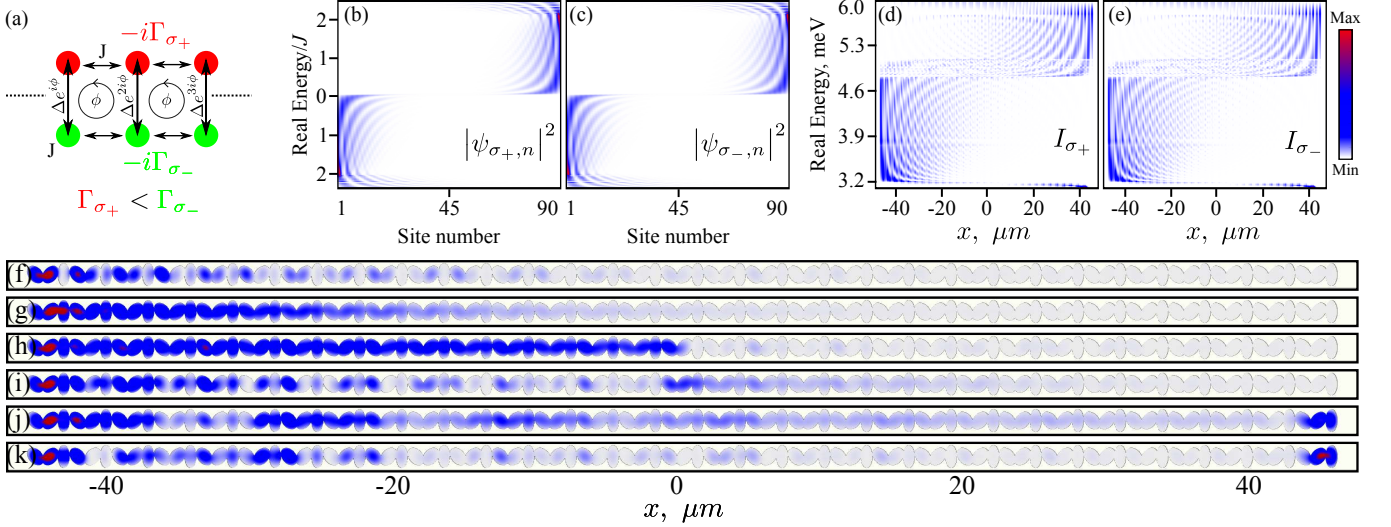


FIG. 5: (a) Scheme of the non-Hermitian skin effect where the decay rates of σ_{\pm} modes are different. (b-c) Mode localization using the tight binding model in Eq. (3). (d-e) Plot of $I_{\sigma_{\pm}}(x)$ for each eigen mode calculated from Eq. (2), which shows the mode localization. Polariton propagation at $t = 200$ ps under a coherent pump when the pump is positioned at the left end (f-g), middle (h-i) and the right end of the chain (j-k). (f,h,i) correspond to $|\psi_{\sigma_{+}}|^2$ and (g,i,k) correspond to $|\psi_{\sigma_{-}}|^2$. Parameters: (b-c) $\Delta/J = 1$, $\Gamma_{\sigma_{+}}/J = 0$, $\Gamma_{\sigma_{-}}/J = 0.3$. (d-e) $P_{\sigma_{+}} = 1.4\Gamma$, $P_{\sigma_{-}} = 0$. All other parameters are the same as those in Fig. 4.

skin effect. The group velocity of the σ_{+} modes decides the localization end of the bands and if one considers the case, where $\Gamma_{\sigma_{+}} > \Gamma_{\sigma_{-}}$, the localization is in the opposite end (see movie2 [70]).

In order to verify our claim, we introduce a spatially uniform σ_{+} incoherent pump, which corresponds to $P_{\sigma_{+}} > 0$ and $P_{\sigma_{-}} = 0$ in Eq. (2) [88, 89]. The main purpose of the incoherent pump is to decrease the effective decay rate of the σ_{+} polaritons, while keeping the system below the condensation threshold. We define, $I_{\sigma_{\pm}}(x) = \int |\psi_{\sigma_{\pm}}^E|^2 dy$, for each eigenstate $\psi_{\sigma_{\pm}}^E$ and plot it as a function of the real energies and the x axis in order to see the localization of the eigenstates corresponding to a finite chain (see Fig. 5(d-e)). Next we inject the polaritons using the same coherent pump as in the TSHE case. In Fig. 5(f-g) the coherent pump is positioned at the left end of the chain, which shows that the polaritons do not propagate from left to right even after 200 ps. Next the coherent pump is positioned at the middle of the chain in Fig. 5(h-i) and unlike the TSHE both σ_{\pm} polaritons propagate leftward. Finally in Fig. 5(j-k) the coherent pump is positioned at the right end of the chain, where σ_{\pm} polaritons propagate from right end to left end and gets accumulated at the left end. This shows that the

one-way propagation of the polaritons is independent of the position of injection. The full dynamics of the polaritons is shown in movie3 [70].

Conclusion.— We have presented a scheme based on an elliptical micropillar chain, where the naturally present polarization splitting inside the micropillars along with their orientation give rise to the topological Spin Hall effect, where σ_{\pm} polaritons propagate in the opposite direction. By making the decay rates of σ_{\pm} polaritons different, the topological phase changes from topological spin Hall effect to non-Hermitian skin effect, where the polaritons accumulate at one end of the chain independent of the excitation position. The energy window in which these effects take place is around 1.5 meV, which is about one order magnitude larger than that of the edge states of the two dimensional topological polariton system. Although, we have used coherent excitation for injecting polaritons into the system, it is possible to set the strength of the circularly polarized spatially uniform incoherent pump above the condensation threshold [70]. For such a case the condensation spontaneously forms at the end of the chain. Because the incoherent pump is distributed over the whole sample, it can in principle help to overcome the problem of having condensation in

some of the modern samples, where the sample burns out before reaching the condensation threshold.

Acknowledgment.— We thank Christian Schneider and

Sebastian Klemmt for stimulating discussions. The work was supported by the Ministry of Education, Singapore (Grant No. MOE2019-T2-1-004).

-
- [1] K. v. Klitzing, G. Dorda, and M. Pepper, New Method for High-Accuracy Determination of the Fine-Structure Constant Based on Quantized Hall Resistance, *Phys. Rev. Lett.* **45**, 494 (1980).
- [2] F. D. M. Haldane, Model for a Quantum Hall Effect without Landau Levels: Condensed-Matter Realization of the “Parity Anomaly”, *Phys. Rev. Lett.* **61**, 2015 (1988).
- [3] C. L. Kane and E. J. Mele, Quantum Spin Hall Effect in Graphene, *Phys. Rev. Lett.* **95**, 226801 (2005).
- [4] W. Han, R. K. Kawakami, M. Gmitra, and J. Fabian, Graphene spintronics, *Nat. Nanotech.* **9**, 794 (2014).
- [5] Z. Wang, Y. D. Chong, J. D. Joannopoulos, and M. Soljačić, Reflection-Free One-Way Edge Modes in a Gyromagnetic Photonic Crystal, *Phys. Rev. Lett.* **100**, 013905 (2008).
- [6] Z. Wang, Y. Chong, J. D. Joannopoulos, and M. Soljačić, Observation of unidirectional backscattering-immune topological electromagnetic states, *Nature* **461**, 772 (2009).
- [7] L. Lu, J. D. Joannopoulos, and M. Soljačić, Topological photonics, *Nat. Photonics* **8**, 821 (2014).
- [8] T. Ozawa, H. M. Price, A. Amo, N. Goldman, M. Hafezi, L. Lu, M. C. Rechtsman, D. Schuster, J. Simon, O. Zilberberg, , and I. Carusotto, Topological photonics, *Rev. Mod. Phys.* **91**, 015006 (2019).
- [9] Y. Yang, Z. Gao, H. Xue, L. Zhang, M. He, Z. Yang, R. Singh, Y. Chong, B. Zhang, and H. Chen, Realization of a three-dimensional photonic topological insulator, *Nature* **565**, 622 (2019).
- [10] Z. Yang, F. Gao, X. Shi, X. Lin, Z. Gao, Y. Chong, and B. Zhang, Topological Acoustics, *Phys. Rev. Lett.* **114**, 114301 (2015).
- [11] B. Y. Xie, H. F. Wang, H. X. Wang, X. Y. Zhu, J. H. Jiang, M. H. Lu, and Y. F. Chen, Second-order photonic topological insulator with corner states, *Phys. Rev. B* **98**, 205147 (2018).
- [12] B. Xie, G. Su, H. F. Wang, F. Liu, L. Hu, S. Y. Yu, P. Zhan, M. H. Lu, Z. Wang, and Y. F. Chen, Higher-order quantum spin Hall effect in a photonic crystal, *Nat. Commun.* **11**, 3768 (2020).
- [13] H. Xue, Y. Yang, F. Gao, Y. Chong, and B. Zhang, Acoustic higher-order topological insulator on a kagome lattice, *Nat. Mater.* **18**, 108 (2019).
- [14] H. Xue, Y. Yang, G. Liu, F. Gao, Y. Chong, and B. Zhang, Realization of an Acoustic Third-Order Topological Insulator, *Phys. Rev. Lett.* **122**, 244301 (2019).
- [15] H. Xue, Y. Ge, H. X. Sun, Q. Wang, D. Jia, Y. J. Guan, S. Q. Yuan, Y. Chong, and B. Zhang, Observation of an acoustic octupole topological insulator, *Nat. Commun.* **11**, 2442 (2020).
- [16] A. B. Khanikaev, S. H. Mousavi, W. K. Tse, M. Kargarian, A. H. MacDonald, and G. Shvets, Photonic topological insulators, *Nat. Mater.* **12**, 233 (2013).
- [17] M. Hafezi, E. A. Demler, M. D. Lukin, and J. M. Taylor, Robust optical delay lines with topological protection, *Nat. Phys.* **7**, 907 (2011).
- [18] G. Q. Liang and Y. D. Chong, Optical Resonator Analog of a Two-Dimensional Topological Insulator, *Phys. Rev. Lett.* **110**, 203904 (2013).
- [19] A. Dutt, Q. Lin, L. Yuan, M. Minkov, M. Xiao, and S. Fan, A single photonic cavity with two independent physical synthetic dimensions, *Science* **367**, 59 (2020).
- [20] T. Ma and G. Shvets, All-Si valley-Hall photonic topological insulator, *New. J. Phys.* **18**, 025012 (2016).
- [21] J. Noh, S. Huang, K. P. Chen, and M. C. Rechtsman, Observation of Photonic Topological Valley Hall Edge States, *Phys. Rev. Lett.* **120**, 063902 (2018).
- [22] Y. Yang, Y. Yamagami, X. Yu, P. Pitchappa, J. Webber, B. Zhang, M. Fujita, T. Nagatsuma, and R. Singh, Terahertz topological photonics for on-chip communication, *Nat. Photonics* **14**, 446 (2020).
- [23] S. Yao and Z. Wang, Edge States and Topological Invariants of Non-Hermitian Systems, *Phys. Rev. Lett.* **121**, 086803 (2018).
- [24] V. M. Martinez Alvarez, J. E. Barrios Vargas, and L. E. F. Foa Torres, Non-Hermitian robust edge states in one dimension: Anomalous localization and eigenspace condensation at exceptional points, *Phys. Rev. B* **97**, 121401(R) (2018).
- [25] L. Jin and Z. Song, Incident Direction Independent Wave Propagation and Unidirectional Lasing, *Phys. Rev. Lett.* **121**, 073901 (2018).
- [26] C. H. Lee and R. Thomale, Anatomy of skin modes and topology in non-Hermitian systems, *Phys. Rev. B* **99**, 201103(R) (2019).
- [27] D. S. Borgnia, A. J. Kruchkov, and R. J. Slager, Non-Hermitian Boundary Modes and Topology, *Phys. Rev. Lett.* **124**, 056802 (2020).
- [28] L. Li, C. H. Lee, S. Mu, and J. Gong, Critical non-Hermitian skin effect, *Nat. Commun.* **11**, 5491 (2020).
- [29] M. Z. Hasan and C. L. Kane, *Colloquium*: Topological insulators, *Rev. Mod. Phys.* **82**, 3045 (2010).
- [30] S. Weidemann, M. Kremer, T. Helbig, T. Hofmann, A. Stegmaier, M. Greiter, R. Thomale, and A. Szameit, Topological funneling of light, *Science* **368**, 311 (2020).
- [31] R. W. Keyes, What Makes a Good Computer Device?, *Science* **230**, 138 (1985).
- [32] I. Carusotto and C. Ciuti, Quantum fluids of light, *Rev. Mod. Phys.* **85**, 299 (2013).
- [33] T. Karzig, C. E. Bardyn, N. H. Lindner, and G. Refael, Topological Polaritons, *Phys. Rev. X* **5**, 031001 (2015).
- [34] C. E. Bardyn, T. Karzig, G. Refael, and T. C. H. Liew, Topological polaritons and excitons in garden-variety systems, *Phys. Rev. B* **91**, 161413(R) (2015).
- [35] A. V. Nalitov, D. D. Solnyshkov, and G. Malpuech, Polariton Z Topological Insulator, *Phys. Rev. Lett.* **114**, 116401 (2015).
- [36] D. R. Gulevich, D. Yudin, I. V. Iorsh, and I. A. Shelykh, Kagome lattice from an exciton-polariton perspective, *Phys. Rev. B* **94**, 115437 (2016).
- [37] C. Li, F. Ye, X. Chen, Y. V. Kartashov, A. Ferrando, L. Torner, and D. V. Skryabin, Lieb polariton topological

- insulators, *Phys. Rev. B* **97**, 081103(R) (2018).
- [38] H. Sigurdsson, Y. S. Krivosenko, I. V. Iorsh, I. A. Shelykh, and A. V. Nalitov, Spontaneous topological transitions in a honeycomb lattice of exciton-polariton condensates due to spin bifurcations, *Phys. Rev. B* **100**, 235444 (2019).
- [39] M. Sun, D. Ko, D. Leykam, V. M. Kovalev, and I. G. Savenko, Exciton-Polariton Topological Insulator with an Array of Magnetic Dots, *Phys. Rev. Applied* **12**, 064028 (2019).
- [40] S. Mandal, R. Banerjee, and T. C. H. Liew, One-Way Reflection-Free Exciton-Polariton Spin-Filtering Channel, *Phys. Rev. Applied* **12**, 054058 (2019).
- [41] X. Ma, Y. V. Kartashov, A. Ferrando, and S. Schumacher, Topological edge states of nonequilibrium polaritons in hollow honeycomb arrays, *Opt. Lett.* **45**, 5311 (2020).
- [42] S. Klemmt, T. H. Harder, O. A. Egorov, K. Winkler, R. Ge, M. A. Bandres, M. Emmerling, L. Worschech, T. C. H. Liew, M. Segev, C. Schneider, and S. Höfling, Exciton-polariton topological insulator, *Nature (London)* **562**, 552 (2018).
- [43] Y. V. Kartashov and D. V. Skryabin, Modulational instability and solitary waves in polariton topological insulators, *Optica* **3**, 1228 (2016).
- [44] Y. V. Kartashov and D. V. Skryabin, Bistable Topological Insulator with Exciton-Polaritons, *Phys. Rev. Lett.* **119**, 253904 (2017).
- [45] R. Banerjee, S. Mandal, and T. C. H. Liew, Coupling between Exciton-Polariton Corner Modes through Edge States, *Phys. Rev. Lett.* **124**, 063901 (2020).
- [46] Y. Zhang, Y. V. Kartashov, L. Torner, Y. Li, and A. Ferrando, Nonlinear higher-order polariton topological insulator, *Opt. Lett.* **45**, 4710 (2020).
- [47] C. E. Bardyn, T. Karzig, G. Refael, and T. C. H. Liew, Chiral Bogoliubov excitations in nonlinear bosonic systems, *Phys. Rev. B* **93**, 020502(R) (2016).
- [48] H. Sigurdsson, G. Li, and T. C. H. Liew, Spontaneous and superfluid chiral edge states in exciton-polariton condensates, *Phys. Rev. B* **96**, 115453 (2017).
- [49] S. Mandal, R. Ge, and T. C. H. Liew, Antichiral edge states in an exciton polariton strip, *Phys. Rev. B* **99**, 115423 (2019).
- [50] X. Xu, H. Xu, S. Mandal, R. Banerjee, S. Ghosh, T. C. H. Liew, Interaction induced bi-skin effect in an exciton-polariton system, [arXiv:2102.13285](https://arxiv.org/abs/2102.13285) (2021).
- [51] T. Gao, E. Estrecho, K. Y. Bliokh, T. C. H. Liew, M. D. Fraser, S. Brodbeck, M. Kamp, C. Schneider, S. Höfling, Y. Yamamoto, F. Nori, Y. S. Kivshar, A. G. Truscott, R. G. Dall, and E. A. Ostrovskaya, Observation of non-Hermitian degeneracies in a chaotic exciton-polariton billiard, *Nature* **526**, 554 (2015).
- [52] R. Su, E. Estrecho, D. Biegańska, Y. Huang, M. Wurdack, M. Pieczarka, A. G. Truscott, T. C. H. Liew, E. A. Ostrovskaya, and Q. Xiong, Direct Measurement of a Non-Hermitian Topological Invariant in a Hybrid Light-Matter System, [arXiv:2012.06133](https://arxiv.org/abs/2012.06133) (2021).
- [53] L. Pickup, H. Sigurdsson, J. Ruostekoski, and P. G. Lagoudakis, Synthetic band-structure engineering in polariton crystals with non-Hermitian topological phases, *Nat. Commun.* **11**, 4431 (2020).
- [54] S. Richter, T. Michalsky, C. Sturm, B. Rosenow, M. Grundmann, and R. Schmidt-Grund, Exceptional points in anisotropic planar microcavities, *Phys. Rev. A* **95**, 023836 (2017).
- [55] P. Comaron, V. Shahnazaryan, W. Brzezicki, T. Hyart, and M. Matuszewski, Non-Hermitian topological end-mode lasing in polariton systems, *Phys. Rev. Research* **2**, 022051(R) (2020).
- [56] S. Mandal, R. Banerjee, E. A. Ostrovskaya, and T. C. H. Liew, Nonreciprocal Transport of Exciton Polaritons in a Non-Hermitian Chain, *Phys. Rev. Lett.* **125**, 123902 (2020).
- [57] C. Leyder, M. Romanelli, J. Ph. Karr, E. Giacobino, T. C. H. Liew, M. M. Glazov, A. V. Kavokin, G. Malpuech, and A. Bramati, Observation of the optical spin Hall effect, *Nat. Phys.* **3**, 628 (2007).
- [58] E. Kammann, T. C. H. Liew, H. Ohadi, P. Cilibrizzi, P. Tsotsis, Z. Hatzopoulos, P. G. Savvidis, A. V. Kavokin, and P. G. Lagoudakis, Nonlinear Optical Spin Hall Effect and Long-Range Spin Transport in Polariton Lasers, *Phys. Rev. Lett.* **109**, 036404 (2012).
- [59] K. Lekenta, M. Król, R. Mirek, K. Lempicka, D. Stephan, R. Mazur, P. Morawiak, P. Kula, W. Piecek, P. G. Lagoudakis, B. Pietka, and J. Szczytko, Tunable optical spin Hall effect in a liquid crystal microcavity, *Light Sci. Appl.* **7**, 74 (2018).
- [60] I. A. Shelykh, A. V. Nalitov, and I. V. Iorsh, Optical analog of Rashba spin-orbit interaction in asymmetric polariton waveguides, *Phys. Rev. B* **98**, 155428 (2018).
- [61] A. Fieramosca, L. Polimeno, G. Lerario, L. De Marco, M. De Giorgi, D. Ballardini, L. Dominici, V. Ardizzone, M. Pugliese, V. Maiorano, G. Gigli, C. Leblanc, G. Malpuech, D. Solnyshkov, and D. Sanvitto, Chromodynamics of photons in an artificial non-Abelian magnetic Yang-Mills field, [arXiv:1912.09684](https://arxiv.org/abs/1912.09684) (2019).
- [62] K. Rechcińska, M. Król, R. Mazur, P. Morawiak, R. Mirek, K. Lempicka, W. Bardyszewski, M. Matuszewski, P. Kula, W. Piecek, P. G. Lagoudakis, B. Pietka, and J. Szczytko, Engineering spin-orbit synthetic Hamiltonians in liquid-crystal optical cavities, *Science* **366**, 727 (2019).
- [63] C. E. Whittaker, T. Dowling, A. V. Nalitov, A. V. Yulin, B. Royall, E. Clarke, M. S. Skolnick, I. A. Shelykh, and D. N. Krizhanovskii, Optical analogue of Dresselhaus spin-orbit interaction in photonic graphene, *Nat. Photonics* (2020).
- [64] Z. Zhang, S. Liang, F. Li, S. Ning, Y. Li, G. Malpuech, Y. Zhang, M. Xiao, and D. Solnyshkov, Spin-orbit coupling in photonic graphene, *Optica* **7**, 455 (2020).
- [65] M. Król, H. Sigurdsson, K. Rechcińska, P. Oliwa, K. Tyszka, W. Bardyszewski, A. Opala, M. Matuszewski, P. Morawiak, R. Mazur, W. Piecek, P. Kula, P. G. Lagoudakis, B. Pietka, and J. Szczytko, Observation of second-order meron polarization textures in optical microcavities, *Optica* **8**, 255 (2021).
- [66] J. Ren, Q. Liao, F. Li, Y. Li, O. Bleu, G. Malpuech, J. Yao, H. Fu, and D. Solnyshkov, Non-trivial band geometry in an optically active system, *Nat. Commun.* **12**, 689 (2021).
- [67] P. Kokhanchik, H. Sigurdsson, B. Pietka, J. Szczytko, and P. G. Lagoudakis, Photonic Berry curvature in double liquid crystal microcavities with broken inversion symmetry, *Phys. Rev. B* **103**, L081406 (2021).
- [68] R. Banerjee, T. C. H. Liew, and O. Kyriienko, Realization of Hofstadter's butterfly and a one-way edge mode in a polaritonic system, *Phys. Rev. B* **98**, 075412 (2018).
- [69] S. Gerhardt, M. Deppisch, S. Betzold, T. H. Harder, T.

- C. H. Liew, A. Predojević, S. Höfling, and C. Schneider, Polarization-dependent light-matter coupling and highly indistinguishable resonant fluorescence photons from quantum dot-micropillar cavities with elliptical cross section, *Phys. Rev. B* **100**, 115305 (2019).
- [70] See supplementary materials at [] for further calculations and information about the movies, which includes Refs. [71–87].
- [71] E. Estrecho, T. Gao, N. Bobrovska, D. Comber-Todd, M. D. Fraser, M. Steger, K. West, L. N. Pfeiffer, J. Levinsen, M. M. Parish, T. C. H. Liew, M. Matuszewski, D. W. Snoke, A. G. Truscott, and E. A. Ostrovskaya, Direct measurement of polariton-polariton interaction strength in the Thomas-Fermi regime of exciton-polariton condensation, *Phys. Rev. B* **100**, 035306 (2019).
- [72] M. Vladimirova, S. Cronenberger, D. Scalbert, K. V. Kavokin, A. Miard, A. Lemaître, J. Bloch, D. Solnyshkov, G. Malpuech, and A. V. Kavokin, Polariton-polariton interaction constants in microcavities, *Phys. Rev. B* **82**, 075301 (2010).
- [73] M. O. Borgh, J. Keeling, and N. G. Berloff, Spatial pattern formation and polarization dynamics of a nonequilibrium spinor polariton condensate, *Phys. Rev. B* **81**, 235302 (2010).
- [74] D. Read, T. C. H. Liew, Yuri G. Rubo, and A. V. Kavokin, Stochastic polarization formation in exciton-polariton Bose-Einstein condensates, *Phys. Rev. B* **80**, 195309 (2009).
- [75] T. H. Harder, M. Sun, O. A. Egorov, I. Vakulchyk, J. Beierlein, P. Gagel, M. Emmerling, C. Schneider, U. Peschel, I. G. Savenko, S. Klemmt, S. Höfling, Coherent topological polariton laser, [arXiv:2005.14546](https://arxiv.org/abs/2005.14546) (2020).
- [76] A. Amo, T. C. H. Liew, C. Adrados, R. Houdré, E. Giacobino, A. V. Kavokin, and A. Bramati, Exciton-polariton spin switches, *Nat. Photonics* **4**, 361 (2010).
- [77] T. Gao, C. Antón, T. C. H. Liew, M. D. Martín, Z. Hatzopoulos, L. Viña, P. S. Eldridge, and P. G. Savvidis, Spin selective filtering of polariton condensate flow, *Appl. Phys. Lett.* **107**, 011106 (2015).
- [78] C. Antón, S. Morina, T. Gao, P. S. Eldridge, T. C. H. Liew, M. D. Martín, Z. Hatzopoulos, P. G. Savvidis, I. A. Shelykh, and L. Viña, Optical control of spin textures in quasi-one-dimensional polariton condensates, *Phys. Rev. B* **91**, 075305 (2015).
- [79] A. Opala, S. Ghosh, T. C.H. Liew, and M. Matuszewski, Neuromorphic Computing in Ginzburg-Landau Polariton-Lattice Systems, *Phys. Rev. Applied* **11**, 064029 (2019).
- [80] D. Ballarini, A. Gianfrate, R. Panico, A. Opala, S. Ghosh, L. Dominici, V. Ardizzone, M. De Giorgi, G. Lerario, G. Gigli, T. C. H. Liew, M. Matuszewski, and D. Sanvitto, Polaritonic Neuromorphic Computing Outperforms Linear Classifiers, *Nano Lett.* **20**, 3506 (2020).
- [81] H. Xu, S. Ghosh, M. Matuszewski, and T. C.H. Liew, Universal Self-Correcting Computing with Disordered Exciton-Polariton Neural Networks, *Phys. Rev. Applied* **13**, 064074 (2020).
- [82] R. Mirek, A. Opala, P. Comaron, M. Furman, M. Król, K. Tyszka, B. Seredynski, D. Ballarini, D. Sanvitto, T. C. H. Liew, W. Pacuski, J. Suffczynski, J. Szczytko, M. Matuszewski, and B. Pietka, Neuromorphic Binarized Polariton Networks, *Nano Lett.* (2021).
- [83] D. Ballarini, M. De Giorgi, E. Cancellieri, R. Houdré, E. Giacobino, R. Cingolani, A. Bramati, G. Gigli, and D. Sanvitto, All-optical polariton transistor, *Nat. Commun.* **4**, 1778 (2013).
- [84] X. Ma, B. Berger, M. Aßmann, R. Driben, T. Meier, C. Schneider, S. Höfling, and S. Schumacher, Realization of all-optical vortex switching in exciton-polariton condensates, *Nat. Commun.* **11**, 897 (2020).
- [85] C. Antón, T. C. H. Liew, D. Sarkar, M. D. Martín, Z. Hatzopoulos, P. S. Eldridge, P. G. Savvidis, and L. Viña, Operation speed of polariton condensate switches gated by excitons, *Phys. Rev. B* **89**, 235312 (2014).
- [86] C. Antón, T. C. H. Liew, G. Tosi, M. D. Martín, T. Gao, Z. Hatzopoulos, P. S. Eldridge, P. G. Savvidis, and L. Viña, Dynamics of a polariton condensate transistor switch, *Appl. Phys. Lett.* **101**, 261116 (2012).
- [87] H. Flayac and I. G. Savenko, An exciton-polariton mediated all-optical router, *Appl. Phys. Lett.* **103**, 201105 (2013).
- [88] N. Carlon Zambon, P. St-Jean, M. Milićević, A. Lemaître, A. Harouri, L. Le Gratiet, O. Bleu, D. D. Solnyshkov, G. Malpuech, I. Sagnes, S. Ravets, A. Amo, and J. Bloch, Optically controlling the emission chirality of microlasers, *Nat. Photonics* **13**, 283 (2019).
- [89] M. Klaas, O. A. Egorov, T. C. H. Liew, A. Nalitov, V. Marković, H. Suchomel, T. H. Harder, S. Betzold, E. A. Ostrovskaya, A. Kavokin, S. Klemmt, S. Höfling, and C. Schneider, Nonresonant spin selection methods and polarization control in exciton-polariton condensates, *Phys. Rev. B* **99**, 115303 (2019).

Supplemental material for From the topological spin-Hall effect to the non-Hermitian skin effect in an elliptical micropillar chain

S. Mandal,^{*} R. Banerjee,[†] and T.C.H. Liew[‡]

*Division of Physics and Applied Physics, School of Physical and Mathematical Sciences,
Nanyang Technological University, Singapore 637371, Singapore*

I. REALIZATION OF THE COMPLEX HOPPING BETWEEN σ_{\pm} MODES

To show the complex hopping between the σ_{\pm} spin states inside an elliptical micropillar, we consider L and T to be the energies of the modes having linear polarization along the longitudinal (semi-major axis) and transverse (semi-minor axis) directions, respectively. This can be represented as

$$i\hbar \frac{\partial}{\partial t} \begin{bmatrix} \psi_L \\ \psi_T \end{bmatrix} = \begin{bmatrix} L & 0 \\ 0 & T \end{bmatrix} \begin{bmatrix} \psi_L \\ \psi_T \end{bmatrix} = H_{LT} \begin{bmatrix} \psi_L \\ \psi_T \end{bmatrix}, \quad (\text{S1})$$

where

$$H_{LT} = \begin{bmatrix} L & 0 \\ 0 & T \end{bmatrix}. \quad (\text{S2})$$

If the longitudinal axis of the elliptical micropillar makes an angle θ with the x axis, then in the circular polarization basis the system can be represented as

$$i\hbar \frac{\partial}{\partial t} \begin{bmatrix} \psi_{\sigma_+} \\ \psi_{\sigma_-} \end{bmatrix} = M^\dagger H_{LT} M \begin{bmatrix} \psi_{\sigma_+} \\ \psi_{\sigma_-} \end{bmatrix} = \begin{bmatrix} \varepsilon & \Delta e^{2i\theta} \\ \Delta e^{-2i\theta} & \varepsilon \end{bmatrix} \begin{bmatrix} \psi_{\sigma_+} \\ \psi_{\sigma_-} \end{bmatrix}. \quad (\text{S3})$$

Here

$$M = \frac{1}{\sqrt{2}} \begin{bmatrix} e^{-i\theta} & e^{i\theta} \\ -ie^{-i\theta} & ie^{i\theta} \end{bmatrix} \quad (\text{S4})$$

is the transformation matrix, $\varepsilon = (L + T)/2$ represents the onsite energy, and $\Delta = (L - T)/2$ represents the polarization splitting. It shows that σ_{\pm} spin states are coupled with a complex hopping, where an orientation angle θ induces 2θ phase in the hopping term.

II. EXCITON-POLARITON CONDENSATION

In order to show the exciton-polariton condensation, we set the incoherent pumps $P_{\sigma_+} = 2.2\Gamma$ and $P_{\sigma_-} = 0$, which is above the condensation threshold. In this regime the non-linear interaction terms become relevant. Consequently, the dynamics of the polaritons is given by the following non-linear driven dissipative Gross-Pitaevskii equation

$$i\hbar \frac{\partial \psi_{\sigma_{\pm}}}{\partial t} = \left[-(1 - i\lambda) \frac{\hbar^2 \nabla^2}{2m} + V(x, y) + i(P_{\sigma_{\pm}} - \Gamma) + \alpha_1 |\psi_{\sigma_{\pm}}|^2 + \alpha_2 |\psi_{\sigma_{\mp}}|^2 - i\alpha_{\text{NL}} |\psi_{\sigma_{\pm}}|^2 \right] \psi_{\sigma_{\pm}} + V_T(x, y, \theta) \psi_{\sigma_{\mp}}. \quad (\text{S5})$$

Here α_1 and α_2 are the non-linear polariton-polariton interaction coefficients between the same spins and opposite spins, respectively. α_{NL} is the gain saturation caused by the depletion of the excitonic reservoir. We choose $\alpha_1 = 10^{-3}$

^{*}Corresponding author: subhaska001@e.ntu.edu.sg

[†]Corresponding author: rimi001@e.ntu.edu.sg

[‡]Corresponding author: tchliew@gmail.com

meV μm^2 [S1], $\alpha_2 = -0.1\alpha_1$ [S2], and $\alpha_{\text{NL}} = 0.3\alpha_1$ [S3]. A phenomenological parameter $\lambda = 5 \times 10^{-3}$ is introduced to take into account the relaxation process [S4]. This corresponds to higher energy states decaying faster compared to the lower energy states. We keep all other parameters the same as those in the main text and solve the time dynamics in Eq. (S5) using a very small random noise as an initial condition. In Figs. S1(a-b) the intensities of the σ_{\pm} modes are shown, respectively. Although P_{σ_+} is uniformly distributed over the whole lattice, the condensates form at the left end of the lattice due to the non-Hermitian skin effect. In Fig. S1(c) the dispersion corresponding to the condensate is shown, which is slightly blueshifted due to the polariton-polariton interaction. Similar topological edge mode condensation, but based on Hermitian Su-Schrieffer-Heeger polariton lattice has been demonstrated recently [S5].

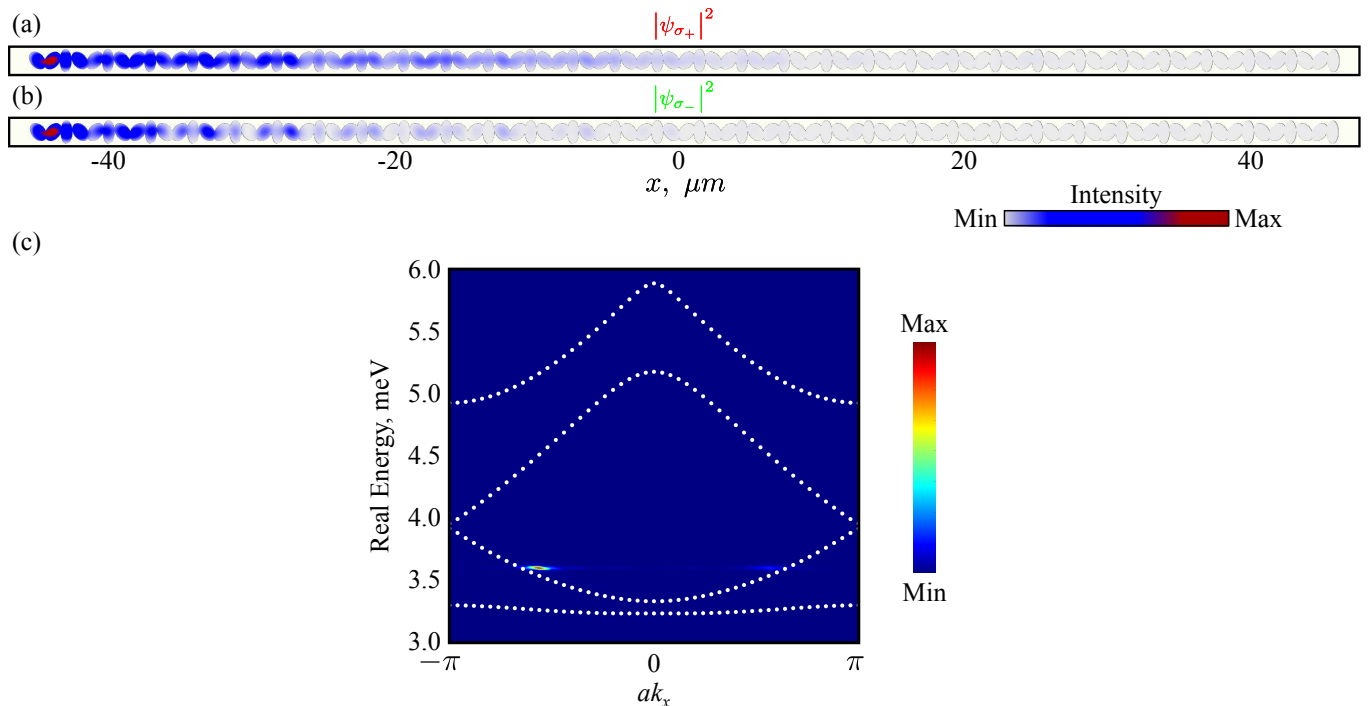


FIG. S1: (a-b) Intensities of the condensate corresponding to the σ_{\pm} modes. (c) Formation of the condensate in the reciprocal space. The dotted curve is the dispersion corresponding to the linear case shown in Fig. 3 in the main text.

III. COMPARISON OF THE POLARITON PROPAGATION UNDER A PULSED EXCITATION

In this section, we compare the dynamics of the polaritons under a pulsed excitation in the topological spin-Hall case and non-Hermitian skin effect case. The dynamics of the polaritons is given by Eq. 2 in the main text, however the coherent continuous pump term is changed to a pulse

$$i\hbar \frac{\partial \psi_{\sigma_{\pm}}}{\partial t} = \left[-\frac{\hbar^2 \nabla^2}{2m} + V(x, y) + i(P_{\sigma_{\pm}} - \Gamma) \right] \psi_{\sigma_{\pm}} + V_T(x, y, \theta) \psi_{\sigma_{\mp}} + F_{\sigma_{\pm}}(x, y) e^{[-(t-t_0)^2/2\tau^2]} e^{i(k_p x - \omega_p t)}. \quad (\text{S6})$$

Here $t_0 = 0$ ps is the time when the pulse is launched and $\tau = 10$ ps is the width of the pulse in time. In Fig. S2 the dynamics of the polaritons is shown. In Figs. S2(a-c) the spin-Hall nature ($P_{\sigma_{\pm}} = 0$) can be seen, where σ_{\pm} polaritons propagate in the opposite directions. When the σ_+ (σ_-) polaritons hit the left (right) end of the chain, they couple with the σ_- (σ_+) polaritons and propagate towards the right (left) end. The whole dynamics is shown in movie1 lower panel.

Next in Figs. S2(d-f) the polariton dynamics in the non-Hermitian skin effect regime ($P_{\sigma_+} = 1.4\Gamma$, $P_{\sigma_-} = 0$) is shown. In this case, both the σ_{\pm} polaritons propagate in the same directions.

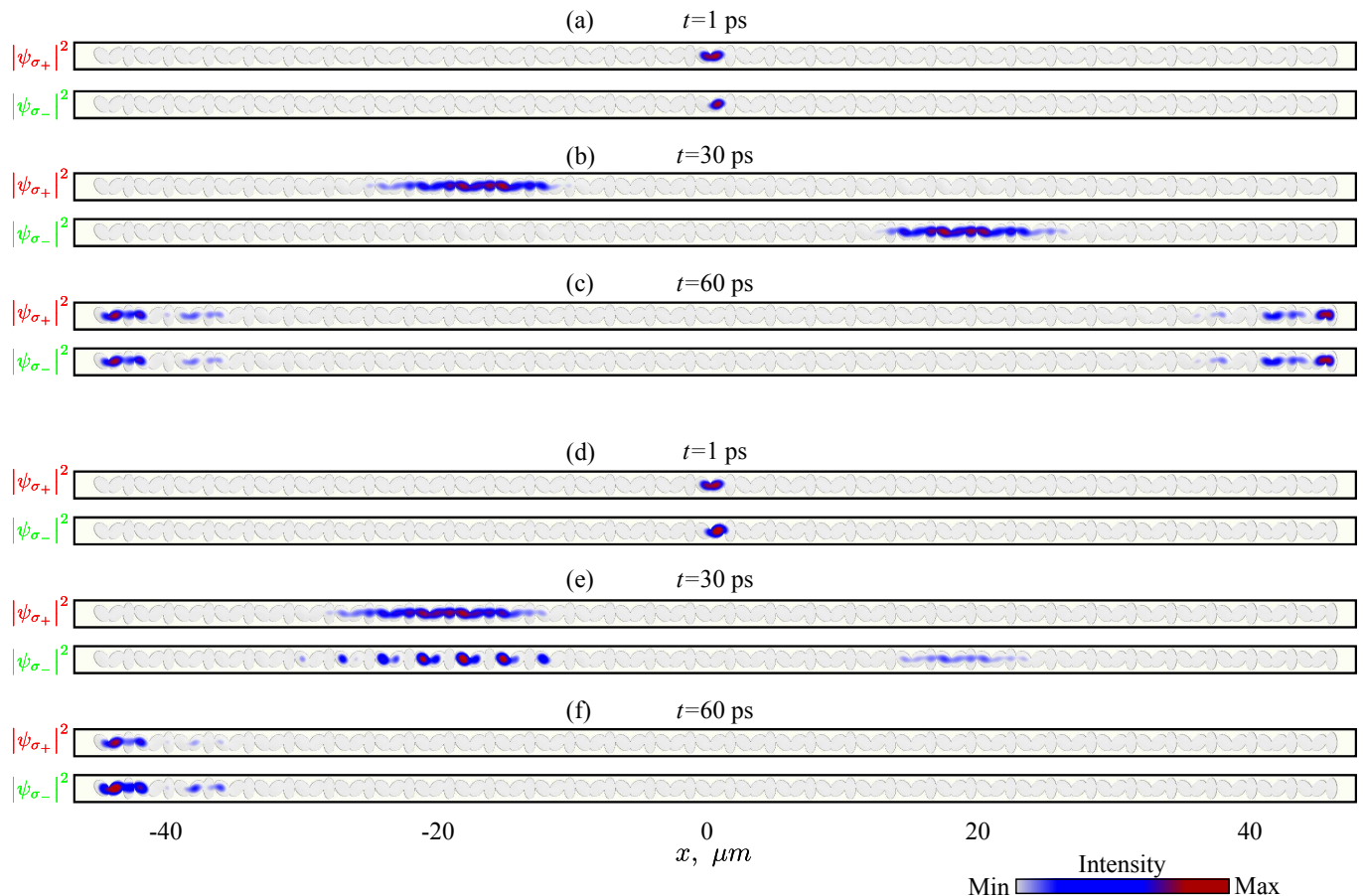


FIG. S2: Polariton propagation under a pulsed excitation showing the topological spin-Hall effect in (a-c) and non-Hermitian skin effect in (d-f).

IV. SUPPLEMENTARY MOVIES

In this section we provide the description of the supplementary movies.

Movie1.— In movie1, we show the topological spin-Hall nature using a linearly polarized continuous coherent pump (upper panel) and a pulse (lower panel). Both the pump and pulse are positioned at the middle of the chain. Under the pulsed excitation the coupling between the opposite circularly polarized modes at the edges of the sample can be seen, where the overall motion is anticlockwise. Such a non-trivial directional dependent motion of the spins, may find its application in connecting different spin-dependent polariton devices [S6, S7, S8].

Movie2.— Movie2 shows the localization of the bands in the tight binding model according to Eq. (3) in the main text. Even a small inequality in the decay rates give rise to the non-Hermitian skin effect. The localization of the modes starts to become more prominent as $|\Gamma_{\sigma_+} - \Gamma_{\sigma_-}|$ increases. When $\Gamma_{\sigma_+} > \Gamma_{\sigma_-}$, the modes get localized at the opposite end to the one for case $\Gamma_{\sigma_+} < \Gamma_{\sigma_-}$.

Movie3.— In movie3, we show the polariton propagation for the non-Hermitian skin effect case ($\Gamma_{\sigma_+} < \Gamma_{\sigma_-}$). In the top panel a linearly polarized continuous coherent pump (the same pump used in the topological spin-Hall case) is placed at the left end of the chain. The polaritons spread a little from the excitation position according to the spatial profiles of skin modes, however they do not propagate from the left end to the right end.

In the middle panel the same pump is positioned at the middle of the chain. At initial times σ_- polaritons tries to propagate towards both the left and right ends, however the modes propagating right decay much faster. As a result large polariton population builds up at the left end at larger time.

In the bottom panel the same pump is positioned at the right end of the chain. Unlike the top panel, polaritons can propagate from the right end to left end and get accumulated at the left end.

This movie shows that polaritons can propagate one-way (right to left) independent of the excitation position, while the propagation in the opposite direction is reduced significantly. Such a one-way motion can be used to suppress

feedback in polariton networks [S9, S10, S11, S12] and connecting different components of a polariton information processing device [S13, S14, S15, S16, S17].

-
- [S1] E. Estrecho, T. Gao, N. Bobrovska, D. Comber-Todd, M. D. Fraser, M. Steger, K. West, L. N. Pfeiffer, J. Levinsen, M. M. Parish, T. C. H. Liew, M. Matuszewski, D. W. Snoke, A. G. Truscott, and E. A. Ostrovskaya, Direct measurement of polariton-polariton interaction strength in the Thomas-Fermi regime of exciton-polariton condensation, *Phys. Rev. B* **100**, 035306 (2019).
- [S2] M. Vladimirova, S. Cronenberger, D. Scalbert, K. V. Kavokin, A. Miard, A. Lemaître, J. Bloch, D. Solnyshkov, G. Malpuech, and A. V. Kavokin, Polariton-polariton interaction constants in microcavities, *Phys. Rev. B* **82**, 075301 (2010).
- [S3] M. O. Borgh, J. Keeling, and N. G. Berloff, Spatial pattern formation and polarization dynamics of a nonequilibrium spinor polariton condensate, *Phys. Rev. B* **81**, 235302 (2010).
- [S4] D. Read, T. C. H. Liew, Yuri G. Rubo, and A. V. Kavokin, Stochastic polarization formation in exciton-polariton Bose-Einstein condensates, *Phys. Rev. B* **80**, 195309 (2009).
- [S5] T. H. Harder, M. Sun, O. A. Egorov, I. Vakulchyk, J. Beierlein, P. Gagel, M. Emmerling, C. Schneider, U. Peschel, I. G. Savenko, S. Klemmt, S. Höfling, Coherent topological polariton laser, [arXiv:2005.14546](https://arxiv.org/abs/2005.14546) (2020).
- [S6] A. Amo, T. C. H. Liew, C. Adrados, R. Houdré, E. Giacobino, A. V. Kavokin, and A. Bramati, Exciton-polariton spin switches, *Nat. Photonics* **4**, 361 (2010).
- [S7] T. Gao, C. Antón, T. C. H. Liew, M. D. Martín, Z. Hatzopoulos, L. Viña, P. S. Eldridge, and P. G. Savvidis, Spin selective filtering of polariton condensate flow, *Appl. Phys. Lett.* **107**, 011106 (2015).
- [S8] C. Antón, S. Morina, T. Gao, P. S. Eldridge, T. C. H. Liew, M. D. Martín, Z. Hatzopoulos, P. G. Savvidis, I. A. Shelykh, and L. Viña, Optical control of spin textures in quasi-one-dimensional polariton condensates, *Phys. Rev. B* **91**, 075305 (2015).
- [S9] A. Opala, S. Ghosh, Timothy C.H. Liew, and M. Matuszewski, Neuromorphic Computing in Ginzburg-Landau Polariton-Lattice Systems, *Phys. Rev. Applied* **11**, 064029 (2019).
- [S10] D. Ballarini, A. Gianfrate, R. Panico, A. Opala, S. Ghosh, L. Dominici, V. Ardizzone, M. De Giorgi, G. Lerario, G. Gigli, T. C. H. Liew, M. Matuszewski, and D. Sanvitto, Polaritonic Neuromorphic Computing Outperforms Linear Classifiers, *Nano Lett.* **20**, 3506 (2020).
- [S11] H. Xu, S. Ghosh, M. Matuszewski, and T. C.H. Liew, Universal Self-Correcting Computing with Disordered Exciton-Polariton Neural Networks, *Phys. Rev. Applied* **13**, 064074 (2020).
- [S12] R. Mirek, A. Opala, P. Comaron, M. Furman, M. Król, K. Tyszka, B. Serebnyński, D. Ballarini, D. Sanvitto, T. C. H. Liew, W. Pacuski, J. Suffczynski, J. Szczytko, M. Matuszewski, and B. Pietka, Neuromorphic Binarized Polariton Networks, *Nano Lett.* (2021).
- [S13] D. Ballarini, M. De Giorgi, E. Cancellieri, R. Houdré, E. Giacobino, R. Cingolani, A. Bramati, G. Gigli, and D. Sanvitto, All-optical polariton transistor, *Nat. Commun.* **4**, 1778 (2013).
- [S14] C. Antón, T. C. H. Liew, D. Sarkar, M. D. Martín, Z. Hatzopoulos, P. S. Eldridge, P. G. Savvidis, and L. Viña, Operation speed of polariton condensate switches gated by excitons, *Phys. Rev. B* **89**, 235312 (2014).
- [S15] C. Antón, T. C. H. Liew, G. Tosi, M. D. Martín, T. Gao, Z. Hatzopoulos, P. S. Eldridge, P. G. Savvidis, and L. Viña, Dynamics of a polariton condensate transistor switch, *Appl. Phys. Lett.* **101**, 261116 (2012).
- [S16] H. Flayac and I. G. Savenko, An exciton-polariton mediated all-optical router, *Appl. Phys. Lett.* **103**, 201105 (2013).
- [S17] X. Ma, B. Berger, M. Aßmann, R. Driben, T. Meier, C. Schneider, S. Höfling, and S. Schumacher, Realization of all-optical vortex switching in exciton-polariton condensates, *Nat. Commun.* **11**, 897 (2020).